Perovskite Solar Cells

Juvinch R. Vicente and Jixin Chen
Department of Chemistry and Biochemistry, Nanoscale and Quantum Phenomena Institute, Ohio University, Athens, Ohio, U.S.A.

Abstract
Solar energy is projected to be one of the ultimate sustainable energy resources. Solar cells are devices that directly convert photon energy into electricity. One of the emerging techniques is perovskite solar cells (PSCs), which have already shown a great promise in its infancy stage. This entry discusses a brief overview of PSCs, including operation and critical material properties, the general fabrication methods employed in laboratory scale, the feasible upscaling fabrication methods currently being investigated, and finally, the existing challenges and opportunities of this technology.

Keywords
Solar energy
Organic-inorganic hybrid perovskite
Thin-film photovoltaic devices
Power conversion efficiency

INTRODUCTION

Perovskite solar cells (PSCs) is considered as a promising candidate for future cost-effective photovoltaics. The key component in a PSC is a thin-layer of organic-inorganic hybrid perovskite (OHP), which has excellent properties in optical absorption and charge transport, and is compatible with low-cost solution-based processing. OHPs were initially demonstrated in 2009 by Miyasaka as the sensitizers for a mesoporous photoelectrode in dye-sensitized solar cells (DSSCs), with a minimal power conversion efficiency (PCE) of 3.8%, and a poor stability due to the liquid-based electrolytes. In 2012, all-solid-state PSC with much improved stability and PCE was introduced by Park and Graetzel. In 2013, Snaith further demonstrated that OHPs can be operated as an efficient absorber layer in planar architectures. Since then, rapid progress has been achieved for PSCs with PCE now reaching over 22% in the middle of 2017, and more than one-year stability with over 11.2% PCE for 100 cm^2 modules in the early 2017.

SOLAR CELL WORKING PRINCIPLE

Solar cells are devices that facilitate the conversion of sunlight directly into electrical energy. The main processes involved in solar cell operations generally include (with an example of PSC given in Fig. 1):[1]

1. Generation of free-charge carriers (electrons and holes) in the absorber layer after light absorption.
2. Transportation of the free-charge carriers to their respective electrodes through selective interfaces for either electrons or holes.
3. Collection of the free-charge carriers in the electrodes, which provides power to an external load.

The energy generated from solar cells are derived from the photons coming from the sun. According to the Planck-Einstein relation, the energy of a single photon is expressed as:

$$E_{ph} = \frac{hc}{\lambda}$$

Where: h is the Planck's constant, c is the speed of light in vacuum, λ is the wavelength of photons.

In most cases, E_{ph} is expressed in terms of electron-volts (eV) since the values in joules are too small (1 eV = 1.602×10^{-19} J). The energy of the majority of photons coming from the sun ranges from 0.5 to 4 eV originated from the black-body radiation of a solar surface temperature of ~5800 K.[2] The actual distribution is dependent on variables such as time of the day, altitude, and atmospheric conditions due to the absorption and scattering of the atmosphere. In testing solar cells, AM1.5G spectrum is often used as a standard, which integrates to 1000 W/m^2 of total energy flux.[3]

Encyclopedia of Chemical Processing
DOI: 10.1081/E-ECHP-140000328

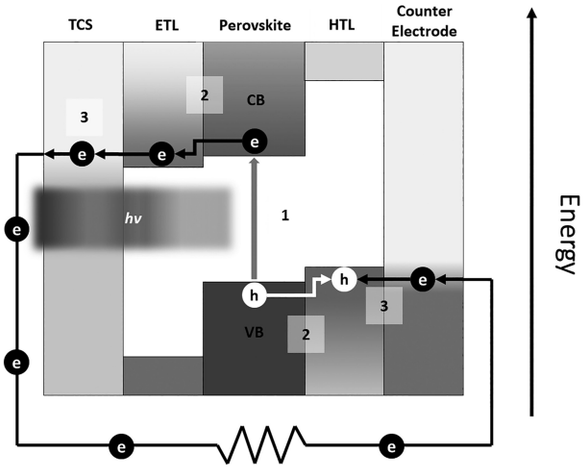

Fig. 1 Basic processes involved in the photovoltaic conversion of solar energy ($h\nu$) to electrical energy in a PSC. TCS, transparent conductive substrates; ETL, electron transport layer; HTL, hole transport layer; CB, conduction band; VB, valence band.

The number of free-charge carriers or *photocurrent* generated within the absorber layer depends mainly on its bandgap (E_g), that is the energy difference between its ground (valence band of a semiconductor) and excited (conduction band) states. Ideally, only photons with energies equal or higher than the bandgap get absorbed ($E_{ph} \geq E_g$) to produce free-charge carriers, while photons with lower energies are transmitted. In principle, the lower the bandgap, the higher the photocurrent. However, bandgap also restricts the energy of each free-charge carrier or its *photovoltage*, and the higher the bandgap, the higher is the photovoltage.[4] The electrical energy per unit solar cell area is the product of the photocurrent and the photovoltage, E_e = IV/area (W/m^2).[2] The solar efficiency is defined the electrical energy over the total solar energy received by the solar cell: PCE ≡ E_e/1000 for the AM1.5G spectrum. The PCE limit of a single p-n junction under AM1.5G has been calculated to be the Shockley–Queisser limit, 33.7% with a bandgap of 1.34 eV.[2] Thus, the optimum bandgap of absorber materials used in solar cells ranges between 1 and 1.5 eV to approach the best condition of this limit. Table 1 summarizes the bandgap of photovoltaic materials including perovskites used in existing PV technologies and their reference record PCE.

To generate photocurrent, the free electrons and holes have to be transported and collected through their respective electrodes, otherwise, they will eventually recombine in the absorber layer, in which case the energy they carry is lost into heat and/or emission.[10] In PSCs, charge transports are achieved by *electron transport layer* (ETL) and *hole transport layer* (HTL) (Fig. 1). ETL is made of *n*-type semiconductor materials that has high conductivity towards electrons, allowing electrons to flow to the cathode while effectively blocking holes. On the other side of the device, HTL is made of *p*-type semiconductor, allowing the holes to flow to the anode while effectively blocking the flow of electrons, due to its high conductivity towards holes.[11]

Table 1 Photovoltaic semiconductors employed in various single-junction PV technologies with their typical bandgaps and the PCE records for a 1-cm^2 cell

Material	Bandgap (eV)	Efficiency (%)
Silicon	1.12[5]	26.7[6]
GaAs	1.42[5]	28.8[6]
CIGS	1.0–2.4[5]	21.7[6]
CdTe	1.43[5]	21.0[6]
CZTS	1.0–1.6[5]	10.0[6]
Organic	1.0–2.1[7]	11.2[6]
DSSC	1.50–2.5	11.9[6]
Perovskite	1.25–2.23[8,9]	19.7[6]

DEVICE ARCHITECTURE

Perovskite solar cell (PSC) was initially developed based on dye-sensitized solar cell architecture; then planar thin film device architecture was later adapted. Until now, mesoscopic scaffolds and planar heterojunctions are still the two major architectures (Fig. 2). In mesoscopic architectures, the scaffold can be active in electron transport (in sensitized mesoporous structure, Fig. 2A), or completely insulating (in meso-superstructured solar cells, Fig. 2B) that are not involved in charge transport. Planar architecture can be either conventional or inverted depending on the relative positions of the component layers (Fig. 2C and D).

Sensitized Mesoporous-TiO_2 Structure

OHPs were initially incorporated as a sensitizer in dye-sensitized solar cells (Fig. 2A).[12] In this architecture, nanoparticles of $MAPbI_3$ and $MAPbBr_3$ were infiltrated into the mesoporous TiO_2, with a liquid electrolyte hole transport layer, achieving a champion PCE of 3.8% with high optical absorption.[12] One of the major drawbacks of this architecture is the associated poor stability, due to the dissolution of perovskite layer to the liquid electrolyte.[13] To address this issue, the liquid electrolyte was replaced with solid-state hole transport material, 2,2′,7,7′-tetrakis (N,N′-di-p-methoxyphenylamine)-9,9′-spirobifluorene (spiro-OMeTAD), which greatly improved the PCE to 9%, and more importantly the stability of the device.[14] To this date, this solid-state hole transport material is still exceptional in achieving high performance PSCs.

Meso-superstructured Solar Cells (MSSCs)

In 2012, Snaith et al. replaced the mesoporous TiO_2 (m-TiO_2) from DSSC with a wide bandgap and insulating mesoporous alumina (m-Al_2O_3) that is deposited onto a thin compact TiO_2

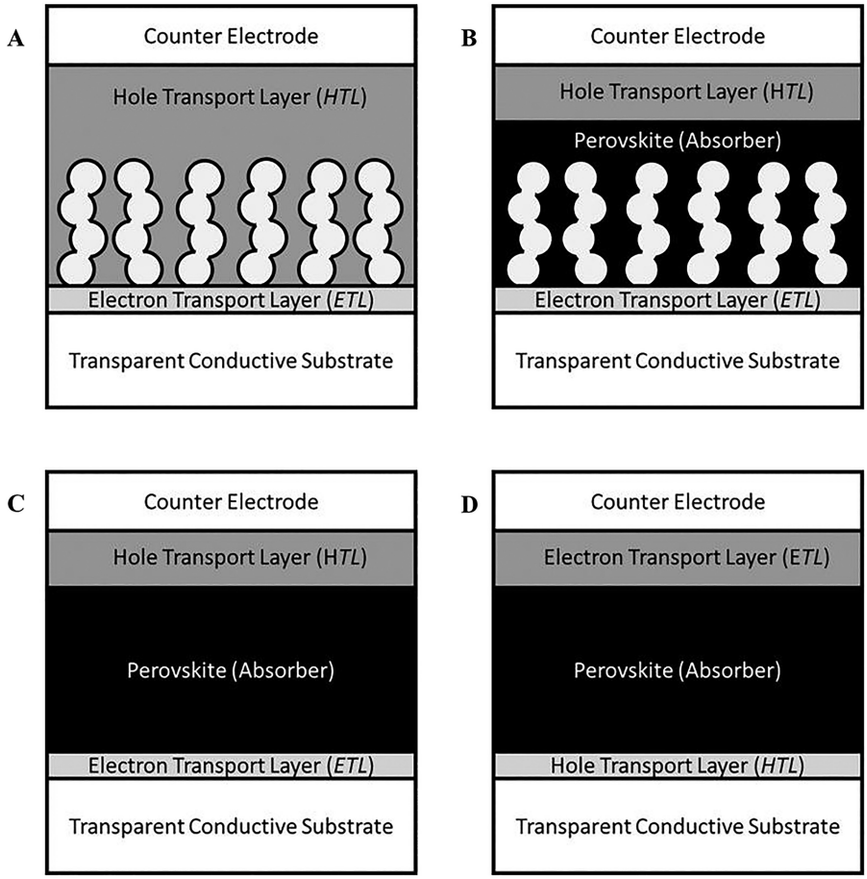

Fig. 2 Schematic diagrams of architectures employed in PSCs. (A) Sensitized-mesoporous scaffold, (B) meso-superstructured architecture, (C) conventional planar architecture, (D) inverted planar architecture.

film on FTO substrate. This new architecture was referred to as meso-superstructured solar cells (MSSCs) (Fig. 2B). Their measurements revealed that the charge transport using m-Al_2O_3 structure was faster by a factor >10^1 compared to the m-TiO_2 based devices. In this report, they concluded that the mesoporous structure does not serve a significant role for charge transport in the device. Rather, it simply acts as a scaffold in which the perovskite is structured.[15]

Planar Heterojunction

By completely removing the mesoporous scaffold, it was demonstrated that OHP can be incorporated to a much simpler planar architecture (Fig. 2C). Before optimization, this architecture initially delivered a PCE of ~5%.[16] The planar architecture was further improved by fabricating the perovskite material via vapor-deposition methods, as a means of creating uniform flat films of the mixed halide perovskite $CH_3NH_3PbI_{3-x}Cl_x$.[17] By obtaining a highly uniform compact perovskite layer, the PCE of planar architecture PSCs was raised to over 15%. The planar architecture gets rid of the infiltration problems of the perovskite and hole transport material in the mesoporous scaffold, which improves the device reproducibility.[18] Early reports in planar PSCs emphasize a uniform and compact perovskite layer for high device PCE, which triggered the development of various deposition techniques.[18,19]

MATERIALSPerovskite Absorber Layer

General structure, ABX_3

Perovskite is the crystal structure name of a calcium titanium oxide mineral composed of calcium titanate ($CaTiO_3$).[21] This name is adapted by the solar cell community to specify a group of organic-inorganic hybrid perovskites (OHPs). They have a general formula of ABX_3 with the organic component (**A** = $CH_3NH_3^+$) in the cuboctahedral site (the center of Fig. 3) and inorganic components (**B** = Pb^{2+}, **X** = I^-, Br^-, Cl^-) in the octahedral structure, with metal center and halide corners (Fig. 3).[20] The chemistry of the organic and inorganic components can be altered to allow tuning of its crystal, optical, and electronic properties.[9]

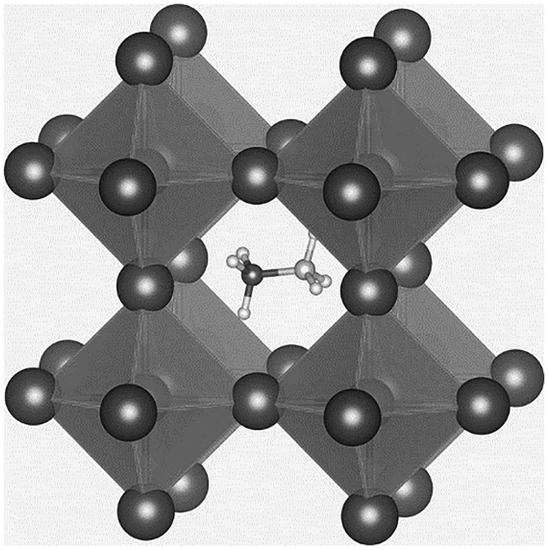

Fig. 3 Crystal structure of a $CH_3NH_3PbX_3$ perovskites (X = I, Br and/or Cl) unit. Eight PbX_6 octahedra trap the methylammonium cation ($CH_3NH_3^+$) in the center.
Source: From Eames et al.[20]

Mixed-metal hybrid perovskites, $AB_{(1-n)}M_nX_3$

Due to ecotoxicity associated to lead (Pb) metal, several efforts have been focused to reduce or completely remove the Pb^{2+} cation. Partially replacing lead (B) with another metal (M) gives a metal cation hybrid-perovskite $\mathbf{AB_{(1-n)}M_nX_3}$. One of the mostly studied alternative to lead is tin(II) cation (Sn^{2+}). An interesting effect of substituting Pb^{2+} with Sn^{2+} is the lowering of the material bandgap (from ~1.7 to ~1.25 eV).[22,23] This makes it possible to design a tandem solar cell where the low-bandgap perovskite based solar cells are the bottom cells, and a wide-bandgap cell is placed on top to further improve the overall PCE.[22] Despite showing comparable PCEs to traditional purely lead-based perovskites, tin-based perovskite suffers from poorer stability because Sn^{2+} is readily oxidized to the more stable Sn^{4+}.

Mixed-halide hybrid perovskites, $ABI_{(3-n)}Y_n$

Substitution of the iodine in ABI_3 to $ABI_{(3-n)}Y_n$ (doping or replacing), where Y is a chlorine or a bromine, changes the properties of the materials and thus the PCE of the PSCs. Earlier studies have shown that introduction of chloride results in an increase in the PCE of PSCs. First-principle calculations initially suggested that the beneficial effect of chloride doping is from the substitution of iodide at the apical positions of the octahedral with chloride.[24] However, the actual concentration and position of the chloride ion in the perovskite structure are still not fully understood.[25] More recently, it has been shown that small amounts of chloride doping (n = 0.05, 5% of total halide) result in a slight bandgap broadening, promotes grain-size growth, and ultimately enhancing the PCE.[26] At larger amounts, the addition of chloride results in the formation of perovskite phase with a wider bandgap that inhibits electron transfer, leading to lowering of the device PCE.[26] Substitution of iodide in ABI_3 crystals with bromide causes the optical bandgap of OHPs to blue shift (larger bandgap) and yields a more cubic perovskite structure.[9] By gradually substituting I^- with Br^- ions, the optical bandgap of OHPs can be continuously tuned from 1.48 to 2.23 eV.[9]

Mixed-cation hybrid perovskites, $A_{(1-n)}C_nBX_3$

Substitution of the organic cation (A) with another cation (C) gives a mixed-cation hybrid perovskites $A_{(1-n)}C_nBX_3$. The most commonly used organic cation in OHPs for solar cell application is methylammonium ($CH_3NH_3^+$, MA^+), and several other organic cations have been already used to prepare OHPs.[27] The suitable sizes of the cation are limited by the rigid and small cuboctahedral cavity formed by the inorganic cage (Fig. 3).[28] Early ab initio theoretical calculations have shown that optical bandgap of OHPs is influenced by the size of the organic cation. Substitution of MA^+ with larger organic cations such as formamidinium ($HN=CHNH_3^+$, FA^+) tends to lower the optical bandgap of perovskite relative to its MA^+ counterpart.[8] By gradually substituting MA^+ with FA^+, the optical bandgap of perovskite could be tuned towards lower values.[27] Pure inorganic-halide perovskites have been prepared by substituting all MA^+ with smaller inorganic cesium cation (Cs^+), resulting in perovskite materials with a larger optical bandgap.[8]

Charge Transport Layers

Elecrtron transport layer (ETL)

In conventional PSCs (Fig. 2C), this layer has to be transparent over the solar spectrum. As such, the most common ETL is a thin compact layer of anatase-TiO_2, mainly due to its wide bandgap of 3.2 eV.[29,30] It is typically deposited on the TCS by spin-coating, dip-coating, and spray pyrolysis of a TiO_2 precursor solution, followed by thermal annealing at high temperatures (450°C–550°C). For inverted PSCs (Fig. 2D), organic ETLs such as [6,6]-phenyl-C60-butyric acid methyl ester (PCBM) are usually used since they do not need to be annealed at very high temperatures, which would otherwise destroy the perovskite layer. Although, recent studies have reported inorganic ETLs prepared at low-temperatures using metal oxide nanoparticles.[31]

Hole transport layer (HTL)

HTL facilitates selective transport of holes from the active layer to the anode, while effectively blocking electrons. The most commonly used HTL in PSCs in normal

architecture (Fig. 2A–C) is a *p*-type organic molecule, 2,2′,7,7′-Tetrakis-(N,N-di-4-methoxyphenylamino)-9,9′-spirobifluorene (spiro-MeOTAD).[32] Spiro-MeOTAD is doped with lithium bis(trifluoromethylsulphonyl)imide (Li-TFSI) to enhance hole mobility and conductivity. It is normally coated onto the active layer by spin-coating its solution (using chlorobenzene as solvent) and allowed to oxidize in dry air or oxygen. In inverted architecture (Fig. 2D), PEDOT:PSS is often used, as well as thin films of amorphous nickel oxide (NiO_x).

Electrodes

Transparent conductive substrates (TCS)

The main purpose of transparent conductive substrates (TCS) is to serve as one of the electrode contacts of the device. In most cases, light enters the solar cell through the supporting substrate. For this reason, the substrate must be transparent over the solar spectrum to minimize the loss of photons before reaching the absorber layer. Typical examples used in PSCs are fluorine-doped tin(II) oxide (FTO) and indium-doped tin(II) oxide (ITO) coated substrates. The substrates could be made of rigid material like glass or flexible like polymer-based materials.[33–35]

Counter electrode

Most commonly used counter metal electrode in PSCs are gold (Au), silver (Ag), aluminum (Al), and platinum (Pt), because of their excellent electrical conductivity. The choice for appropriate counter electrodes is usually based on the alignment of its work function with the valence band of the HTL (or conduction band of ETL for inverted PSCs). With this consideration, Au is usually used for normal PSCs with spiro-MeOTAD as HTL. Recently, more cost-effective alternative counter electrodes based on non-precious metals and carbon materials have also been explored.[36,37]

FABRICATION METHODS

To this date, fabrication of PSCs is still mainly done in the laboratory scale using solution-based processes and vapor-deposition techniques.[17,38–40] The goal mainly is to obtain homogeneous and dense layers of perovskite films that cover the substrate completely. Although not all laboratory scale processes can be translated directly to commercially viable methods, they paved the way to the understanding of the perovskite formation and the materials' critical properties.[41] This served as the basis for the development of feasible upscaling techniques, which are discussed later in this section. In this section, the most commonly used perovskite material, $CH_3NH_3PbI_3$, will be used as an example to describe the techniques. However, the techniques described could be optimized to facilitate fabrication of perovskites with varying compositions as described in earlier sections.

Solution-Based Processes

One of the main advantages of PSCs is their compatibility to solution-based fabrication, which generally translates to cost-effective upscaling methods. Solution-based fabrication of hybrid perovskite can be done by single step deposition or sequential coating of the precursor materials (Fig. 4).[42]

In a single deposition method, equivalent amounts of both precursors (i.e., CH_3NH_3I and PbI_2) are dissolved in a suitable organic solvent, like N,N-dimethylformamide (DMF), dimethyl sulfoxide (DMSO), or γ-butyrolactone. This precursor solution is then spin-coated onto an electrode followed by thermal annealing at about 100°C to evaporate excess solvent and by-products. By convective self-assembly, a dense layer of well-crystallized perovskite material is formed on the substrate.[43] The composition of the precursor solution, the solvent used, the spin-coating parameters, and the thermal annealing conditions are varied to optimize the film properties.[44–46] In two-step solution process, a hot solution of PbI_2 in an organic solvent is spin-coated on the substrate first, followed by thermal annealing to form a uniform PbI_2 thin film layer. Subsequently, the resulting PbI_2 film is exposed to the CH_3NH_3I solution, by dipping or by spin-coating, which leads to the rapid formation of the perovskite film.[38–40]

Vapor-Based Processes

In the earlier stages of solution-based processes, particularly one-step coating methods, perovskite materials

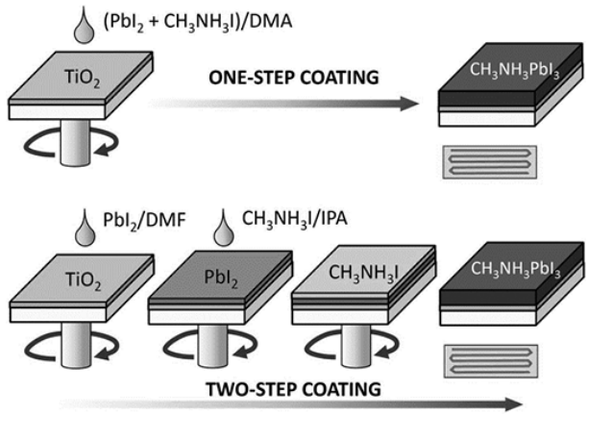

Fig. 4 One-step (A) and two-step (B) sequential deposition of $CH_3NH_3PbI_3$ perovskite. In single step coating, CH_3NH_3I and PbI_2 were mixed in N,N-dimethylacetamide (DMA) and spin-coated on FTO/TiO_2 substrate followed by thermal annealing. In sequential method, a solution of PbI_2 was first coated on the substrate followed by spin-coating of the CH_3NH_3I solution and final annealing treatment.
Source: From Im et al.[38]

deposited on substrates suffered from uncontrolled perovskite formation and large morphological variations between devices.[47] Vapor deposition techniques were later introduced to address this problem.[17] The most commonly used vapor-deposition technique is by co-evaporation. In this method, a clean electrode substrate is placed inside a vacuum chamber at a fixed distance above both precursors (PbI_2 and CH_3NH_3I) that are contained in separate crucibles (Fig. 5).[17] The typical pressure during deposition is about 10^{-5} to 10^{-6} Torr.[48] The precursors are then heated until they evaporate or sublimate. The vapors from both precursors condense on the substrate forming smooth and compact $CH_3NH_3PbI_3$ perovskite layers. The thickness of the forming perovskite film is monitored typically by a quartz crystal microbalance (QCM) mounted inside the vacuum chamber close to the substrate.[48]

UPSCALING METHODS

Feasible upscaling methods for PSCs fabrication are mainly based on solution processes described in the previous section, mainly due to its superior practicability and simplicity over vapor-deposition based processes. Examples of these solution-compatible methods include electrodeposition, spray-coating, inkjet printing, screen printing, and blade coating. Spin-coating, the most commonly used technique at laboratory scale, can be hardly translated to large-scale fabrication because extreme motion is difficult to control and a large amount of material is wasted.[41]

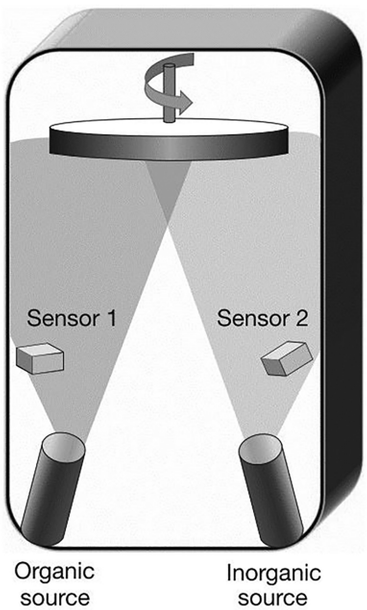

Fig. 5 A schematic diagram of a typical set-up for dual-source co-evaporation of both PbX_2 (inorganic) and CH_3NH_3I (organic) precursor materials.
Source: From Liu et al.[17]

Blade coating

Blade coating refers to a family of coating processes where a liquid layer comes from the shallow channel formed between a stationary blade and moving substrate, or a moving blade and stationary substrate. The well-defined thickness of the resulting film is mainly controlled by the gap between the blade and the substrate.[49] Blade-coating techniques have been widely used in the fabrication of organic solar cells, due to the simplicity of the process and low-cost.[50] In PSCs, blade-coating is based on single-deposition solution process. Several groups have already demonstrated the PSCs with PCE as high as 18.0% using the blade-coating method.[50–52] Blade-coating is not limited to the fabrication of perovskite layer but can be also used to fabricate the ETL and HTL layers.[50,53,54]

Spray coating

Spray coating is an excellent method to obtain large area perovskite thin films at a relatively fast rate. Another advantage of spray coating is that it has been shown to be compatible with the fabrication of charge transport layers (i.e., ETL and HTL) as well.[35,55] The critical parameters for optimizing spray-coating method are the viscosity of the precursor solution, the surface tension, as well as the contact angle of the solution on the substrates, which are dependent on the precursor solution concentration and substrate temperature.[56] The major drawback of spray-coating is the material loss during fabrication.[57] Recently, devices prepared using this technique have been shown to have PCE over 12%.[55]

Screen printing

Screen printing is a technique that deposits a precursor paste/emulsion through a porous printing plate made from woven mesh of synthetic fiber or metal.[58] The application of screen printing on PSC fabrication was mainly an adaptation from DSSCs, where its mainly used to deposit mesoporous TiO_2 layer.[59] In PSCs, mesoporous TiO_2, a mesoporous insulating spacer (typically Al_2O_3 or ZrO_2), and carbon counter electrode are sequentially screen printed and baked before the deposition of the next layer.[60–63] Then, the perovskite precursor solution (single-step deposition or sequential deposition) is infiltrated into the multi-layered mesoporous scaffold followed by thermal annealing at ~100°C.[60–63] Devices based on this technique and architecture have been shown to obtain PCE as high as 15% and stabilities for more than one year under simulated conditions.[63,64]

Electrodeposition

Electrochemical deposition has been used as a versatile technique to produce surface coatings, with the advantages

of precise controllability, low temperature operation, and large-scale production compatibility. Another benefit from electrodeposition is its compatibility to deposit metal oxide charge transport layers such as TiO_2 (*n*-type) and NiO_x (*p*-type).[65,66] In its application to PSCs, PbO thin film is first electrodeposited on the FTO/TiO_2 substrate from an aqueous solution of lead salt (typically lead(II) acetate or nitrate). The resulting PbO thin film is then spin-coated with a layer of the CH_3NH_3I (MAI) solution and heated to allow the formation of the perovskite layer.[67–69] The corresponding overall chemical reaction is shown in Eqs. 1–3. Using this technique, an overall PCE of more than 14% has been already achieved.[68]

$$CH_3NH_3I \leftrightarrow CH_3NH_2 + HI \quad (1)$$

$$PbO + HI \rightarrow PbI_2 + H_2O \quad (2)$$

$$PbI_2 + CH_3NH_3I \rightarrow CH_3NH_3PbI_3 \quad (3)$$

Inkjet printing

Inkjet printing refers to the techniques in which droplets of inks are ejected on a printing substrate to form a pattern.[70] These techniques have the advantage of being material-conserving, especially compared to spin-coating and spray-coating techniques. Inkjet printing is already a commonly used technique in solution-processable organic electronics, making the technique compatible with PSC fabrication.[71,72] In PSCs, reports on inkjet printing are mainly limited to the fabrication of the perovskite layer only, and other layers are prepared using other methods.[73–76] By optimizing the solvents and printing table temperature, Li et al. were able to fabricate PSCs with PCE over 12% using inkjet printing based on single deposition technique.[73] Other inkjet printing techniques based on two-step deposition have been demonstrated as well. For instance, reactive inkjet method (RIJ) was developed where multichannel inkjet printer was used to separately deposit lead salt and organic precursor on the same spot of solid substrates. However, the resulting device had a low PCE of only 0.94%.[74]

CHALLENGES

Despite the promising performance efficiencies, PSCs suffer from rapid undesirable degradation that limits its practical application. These degradation processes are caused by the prolonged exposure to humidity, air, light, and elevated temperatures, which have been shown to undermine chemical structures, optical properties, and ultimately the PCE. Very recently, large area stable perovskite devices have been reported by engineering an ultra-stable 2D/3D $(HOOC(CH_2)_4NH_3)2PbI_4/CH_3NH_3PbI_3$ perovskite junction ($100\,cm^2$) without any performance loss for more than one-year under AM1.5G at 55°C.[64] In addition to these major issues, inconsistencies in current-voltage behavior in PSCs, referred to as hysteresis, creates a problem in accurately measuring the PCE. Finally, lead (Pb^{2+}) in the absorber layer of PSCs have raised environmental and public health concerns due to the associated cytotoxicity.

Long Term Stability

Humidity

Earlier studies suggest that prolonged exposure to humidity and air irreversibly reverts $CH_3NH_3PbI_3$ perovskite to PbI_2 and other Pb^{2+} derivatives (e.g., $PbCO_3$ and PbO).[77,78] Other studies have also shown that water from ambient air (R.H. ≥ 50%) complexes with $CH_3NH_3PbI_3$ perovskite to form hydrated products that reduce the absorption cross section of perovskite in the visible region.[79,80] An evaluation of the effect of ambient air (R.H. = 50–60%) on bromide-substituted $CH_3NH_3PbBr_3$ perovskite suggests that it does not cause significant chemical changes within the material, however, it facilitates crystal growth over time resulting to increase trap-states and detrimental effect on photoluminescence of the material.[81] Great efforts have been made to protect PSC from ambient air through encapsulation and use of metal oxide transport layers.[32,82] However, long-term stability comparable to current commercial photovoltaic devices has not been achieved via encapsulation.

Thermal stability

Thermal instability of PSCs is considered to be a more challenging problem since it is difficult to avoid temperature increase during solar cell operation.[83] Thermal instability of organo-lead halide perovskites originates from phase transition and its organic-inorganic material hybrid nature, where its organic component, methylammonium cation ($CH_3NH_3^+$, MA^+), undergo decomposition leaving behind PbX_2.[83–86] Recent papers have shown that the thermal degradation of $MAPbI_3$ perovskite thin films could occur at temperatures above 85°C,[87] although mixed-halide perovskites have been shown to be more thermally stable.[88] Improvement of thermal stability was also found by replacing MA^+ with a more thermally stable formamidinium cation ($HC(NH_2)_2^+$, FA^+).[9] Another approach is to mix FA^+ with a smaller inorganic cation, cesium (Cs^+), which resulted in more stable perovskite thin films at temperatures above 100°C.[89]

Photostability

Another key challenge to PSCs is their lack of stability over prolonged exposure to solar light. It was earlier showed that prolonged exposure of PSCs to solar irradiation results

to the UV-assisted reduction of photocurrent.[90] Recently, Nie et al. have unveiled that the slow photocurrent degradation of the PSCs is primarily due to the accumulation of light-activated deep-level trap states upon prolonged exposure to solar irradiation, without associated degradation of the perovskite layer.[91] In contrast, Ahn et al. showed that an irreversible photochemical degradation of perovskite is observed when soaked in solar irradiation under humidified air, and suggested that the effect is driven by charges along the perovskite grain boundaries.[92] It is important to note that this detrimental effect is more pronounced on devices using TiO_2 as ETL.[90,92] Recently, it is rationalized that the long-term stability issue is caused by the interfacial degradation because perovskite itself is known to have a good photostability.[93] In mesoporous architectures, this issue was addressed by meso-superstructured devices by replacing the mesoporous TiO_2 with inert mesoporous Al_2O_3.[90] In planar heterojunction devices, this problem could be circumvented by modifying the TiO_2/perovskite interface with fullerene derivatives.[94–96]

Current-Voltage Hysteresis

In solar cells, hysteresis is the change in the current-voltage behavior of a device when measured by forward (negative to positive bias) and reverse (positive to negative bias). This behavior presents a problem in determining the accurate PCE of PSCs. It is proposed that hysteresis emanates from ion-migration within the perovskite layer, as well as interfacial charge recombination, although its exact origin is still being debated.[97–101] Nonetheless, several approaches have already been demonstrated to minimize the hysteretic behavior or PSCs. One approach is to modify the interfaces between the perovskite layer and charge transport layers.[93] A more recent approach by altering the halide composition of the perovskite layer has also shown reduced hysteresis in I-Br mixed-halide perovskite compared to pure-I perovskite.[102]

Environmental Impacts

An environmental benefit of solar cells is the reduced carbon emission compared to traditional fossil fuels. However, the inclusion of lead, which is a water-soluble toxic metal, in PSCs poses potential ecological and public health risks. For this reason, tin-based perovskite materials, as discussed earlier, have been developed. However, life cycle assessments (LCA), accounting processes from raw material extraction to end-of-life of PSCs (PSCs), showed that gold production accounts for the largest environmental impact from PSCs.[103,104] Thus, substitution of gold with silver, aluminum, and carbon-based back electrodes could help mitigate the issue. Nonetheless, among PSC devices considered, the tin-based PSCs showed to have larger environmental impacts compared to lead-based PSC devices due to its lower efficiency and larger amount of materials used (6.4% in this report).[104] Recently, more efficient tin-based devices have been developed with PCE of 17.6%.[22] Due to rapid development in PSCs, updated and more comprehensive LCAs must be done. Moreover, specific architecture, materials used, fabrication method, and overall PCEs must also be carefully considered in designing LCA studies to capture a more consistent and precise evaluation of PSCs environmental impact.

CONCLUSIONS

We have briefly reviewed the PSCs, including the structures of the photovoltaic devices, the materials, and the fabrication methods. Very fast progress has been observed in the past decade in materials screening and modification, architecture design, and fabrication method development. The power conversion efficiency (PCE) of these devices has been improved from <4% to >22% in just several years of development. One-year stable 100 cm^2 modules with >11% PCE have been recently achieved. The research focus moves to extending the lifetime of the high PCE devices or improving the PCE of the stable devices, discovering efficient scaling-up methods, increasing environmental compatibilities, and reducing overall costs.

ACKNOWLEDGEMENT

The authors thank the Ohio University faculty startup fund.

REFERENCES

1. Fonash, S.J. Introduction. . In *Solar Cell Device Physics*; Elsevier Inc.: Burlington, MA, 2010; 1–8.
2. Shockley, W.; Queisser, H.J. Detailed balance limit of efficiency of P-N junction solar cells. J. Appl. Phys. **1961**, *32* (3), 510–519.
3. Gueymard, C.A.; Myers, D.; Emery, K. Proposed reference irradiance spectra for solar energy systems testing. Sol. Energy **2002**, *73* (6), 443–467.
4. Tress, W. Maximum efficiency and open-circuit voltage of perovskite solar cells. In *Organic-Inorganic Halide Perovskite Photovoltaics from Fundamentals to Device Architectures*; Park, N.-G., Grätzel, M., Miyasaka, T., Eds.; Springer International Publishing: Switzerland, 2016; 53–77.
5. Polman, A.; Knight, M.; Garnett, E.C.; Ehrler, B.; Sinke, W.C.; Summary, R.; Polman, A.; Knight, M.; Garnett, E.C.; Ehrler, B.; Sinke, W.C. Photovoltaic materials—Present efficiencies and future challenges. Science **2016**, *352* (6283), 307.
6. Green, M.A.; Hishikawa, Y.; Warta, W.; Dunlop, E.D.; Levi, D.H.; Hohl-Ebinger, J.; Ho-Baillie, A.W.H. Solar cell efficiency tables (version 50). Prog. Photovolt. Res. Appl. **2017**, *25* (7), 668–676.
7. Hou, J.; Guo, X. Active layer materials for organic solar cells. In *Organic Solar Cells*; Springer: London, 2013; 17–42.

8. Stoumpos, C.C.; Malliakas, C.D.; Kanatzidis, M.G. Semiconducting tin and lead iodide perovskites with organic cations: Phase transitions, high mobilities, and near-infrared photoluminescent properties. Inorg. Chem. **2013**, *52* (15), 9019–9038.
9. Eperon, G.E.; Stranks, S.D.; Menelaou, C.; Johnston, M.B.; Herz, L.M.; Snaith, H.J. Formamidinium lead trihalide: A broadly tunable perovskite for efficient planar heterojunction solar cells. Energy Environ. Sci. **2014**, *7* (3), 982.
10. Fonash, S.J. Material properties and device physics basic to photovoltaics. In *Solar Cell Device Physics*; Elsevier Inc.: Burlington, MA, 2010; 9–64.
11. Wurfel, U.; Cuevas, A.; Wurfel, P. Charge carrier separation in solar cells. IEEE J. Photovolt. **2015**, *5* (1), 461–469.
12. Akihiro, K.; Kenjiro, T.; Yasuo, S.; Tsutomu, M. Organometal halide perovskites as visible- light sensitizers for photovoltaic cells. J. Am. Chem. Soc. **2009**, *131* (17), 6050–6051.
13. Zhao, Y.; Zhu, K. Charge transport and recombination in perovskite $(CH_3NH_3)PbI_3$ sensitized TiO_2 solar cells. J. Phys. Chem. Lett. **2013**, *4* (17), 2880–2884.
14. Kim, H.; Lee, C.; Im, J.; Lee, K.; Moehl, T.; Marchioro, A.; Moon, S.; Humphry-baker, R.; Yum, J.; Moser, J.E.; Gratzel, M. Park, N-G. Lead Iodide Perovskite Sensitized All-Solid-State Submicron Thin Film Mesoscopic Solar Cell with Efficiency Exceeding 9%. Sci. Rep. **2012**, 2(591),1–7.
15. Lee, M.M.; Teuscher, J.; Miyasaka, T.; Murakami, T.N.; Snaith, H.J. Efficient hybrid solar cells based on meso-superstructured organometal halide perovskites. Science **2012**, *338* (6107), 643–647.
16. Ball, J.M.; Lee, M.M.; Hey, A.; Snaith, H.J. Low-temperature processed meso-superstructured to thin-film perovskite solar cells. Energy Environ. Sci. **2013**, *6* (6), 1739–1743.
17. Liu, M.; Johnston, M.B.; Snaith, H.J. Efficient planar heterojunction perovskite solar cells by vapour deposition. Nature **2013**, *501* (7467), 395–398.
18. Gamliel, S.; Etgar, L. Organo-metal perovskite based solar cells: Sensitized versus planar architecture. RSC Adv. **2014**, *4* (55), 29012–29021.
19. de Quilettes, D.W.; Vorpahl, S.M.; Stranks, S.D.; Nagaoka, H.; Eperon, G.E.; Ziffer, M.E.; Snaith, H.J.; Ginger, D.S. Impact of microstructure on local carrier lifetime in perovskite solar cells. Science **2015**, *348* (6235), 683–686.
20. Eames, C.; Frost, J.M.; Barnes, P.R.F.; O'Regan, B.C.; Walsh, A.; Islam, M.S. Ionic transport in hybrid lead iodide perovskite solar cells. Nat. Commun. **2015**, *6*, 7497.
21. Wenk, H.-R.; Bulakh, A. *Minerals: Their Constitution and Origin*; Cambridge University Press: New York, 2004.
22. Zhao, D.; Yu, Y.; Wang, C.; Liao, W.; Shrestha, N.; Grice, C.R.; Cimaroli, A.J.; Guan, L.; Ellingson, R.J.; Zhu, K.; Zhao, X.; Xiong, R.-G.; Yan, Y. Low-bandgap mixed tin–lead iodide perovskite absorbers with long carrier lifetimes for all-perovskite tandem solar cells. Nat. Energy **2017**, *2* (4), 17018.
23. Liao, W.; Zhao, D.; Yu, Y.; Shrestha, N.; Ghimire, K.; Grice, C.R.; Wang, C.; Xiao, Y.; Cimaroli, A.J.; Ellingson, R.J.; Podraza, N.J.; Zhu, K.; Xiong, R.G.; Yan, Y. Fabrication of efficient low-bandgap perovskite solar cells by combining formamidinium tin iodide with methylammonium lead iodide. J. Am. Chem. Soc. **2016**, *138* (38), 12360–12363.
24. Mosconi, E.; Amat, A.; Nazeeruddin, M.K.; Grätzel, M.; Angelis, F.De. First Principles modeling of mixed halde organometal perovskites for photovoltaic applications. J. Phys. Chem. **2013**, *117* (27), 13902–13913.
25. Zhang, W.; Saliba, M.; Moore, D.T.; Pathak, S.K.; Horantner, M.T.; Stergiopoulos, T.; Stranks, S.D.; Eperon, G.E.; Alexander-Webber, J.A.; Abate, A.; Sadhanala, A.; Yao, S.; Chen, Y.; Friend, R.H.; Estroff, L.A.; Wiesner, U.; Snaith, H.J. Ultrasmooth organic-inorganic perovskite thin-film formation and crystallization for efficient planar heterojunction solar cells. Nat. Commun. **2015**, *6*, 6142.
26. Xu, F.; Zhang, T.; Li, G.; Zhao, Y. Synergetic effect of chloride doping and $CH_3NH_3PbCl_3$ on $CH_3NH_3PbI_3$–xClx perovskite-based solar cells. ChemSusChem **2017**, *10* (11), 2365–2369.
27. Pellet, N.; Gao, P.; Gregori, G.; Yang, T.-Y.Y.; Nazeeruddin, M.K.; Maier, J.; Grätzel, M. Mixed-organic-cation perovskite photovoltaics for enhanced solar-light harvesting. Angew. Chem. Int. Ed. **2014**, *53* (12), 3151–3157.
28. Borriello, I.; Cantele, G.; Ninno, D. Ab initio investigation of hybrid organic-inorganic perovskites based on tin halides. Phys. Rev. B, Condens. Matter. Mater. Phys. **2008**, *77* (23), 235214.
29. Wu, N.; Wang, J.; Tafen, D.N.; Wang, H.; Zheng, J.-G.; Lewis, J.P.; Liu, X.; Leonard, S.S.; Manivannan, A. Shape-enhanced photocatalytic activity of single-crystalline anatase TiO(2) (101) nanobelts. J. Am. Chem. Soc. **2010**, *132* (19), 6679–6685.
30. Wang, J.; Tafen, D.N.; Lewis, J.P.; Hong, Z.; Manivannan, A.; Zhi, M.; Li, M.; Wu, N. Origin of photocatalytic activity of nitrogen-doped TiO_2 nanobelts. J. Am. Chem. Soc. **2009**, *131* (34), 12290–12297.
31. You, J.; Meng, L.; Song, T.-B.; Guo, T.-F.; Yang, Y.M.; Chang, W.-H.; Hong, Z.; Chen, H.; Zhou, H.; Chen, Q.; Liu, Y.; De Marco, N.; Yang, Y. Improved air stability of perovskite solar cells via solution-processed metal oxide transport layers. Nat. Nanotechnol. **2015**, *11* (1), 1–8.
32. Calió, L.; Kazim, S.; Grätzel, M.; Ahmad, S. Hole-transport materials for perovskite solar cells. Angew. Chem. Int. Ed. **2016**, *55* (47), 14522–14545.
33. Wang, W.-T.; Das, S.K.; Tai, Y. Fully ambient-processed perovskite film for perovskite solar cells: Effect of solvent polarity on lead iodide. ACS Appl. Mater. Interfaces **2017**, *9* (12), 10743–10751.
34. Docampo, P.; Ball, J.M.; Darwich, M.; Eperon, G.E.; Snaith, H.J. Efficient organometal trihalide perovskite planar-heterojunction solar cells on flexible polymer substrates. Nat. Commun. **2013**, *4*, 2761.
35. Zhou, P.; Li, W.; Li, T.; Bu, T.; Liu, X.; Li, J.; He, J.; Chen, R.; Li, K.; Zhao, J.; Huang, F. Ultrasonic spray-coating of large-scale TiO_2 compact layer for efficient flexible perovskite solar cells. Micromachines **2017**, *8* (2), 1–12.
36. Wang, L.; Li, G.-R.; Zhao, Q.; Gao, X.-P. Non-precious transition metals as counter electrode of perovskite solar cells. Energy Storage Mater. **2016**, *7*, 40–47.
37. Yang, Y.Y.; Xiao, J.Y.; Wei, H.Y.; Zhu, L.F.; Li, D.M.; Luo, Y.H.; Wu, H.J.; Meng, Q.B. An all-carbon counter electrode for highly efficient hole-conductor-free organo-metal perovskite solar cells. RSC Adv. **2014**, *4* (95), 52825–52830.

38. Im, J.H.; Kim, H.S.; Park, N.G. Morphology-photovoltaic property correlation in perovskite solar cells: One-step versus two-step deposition of $CH_3NH_3PbI_3$. APL Mater. **2014**, *2* (8), 81510.
39. Ko, H.-S.; Lee, J.-W.; Park, N.-G. 15.76% efficiency perovskite solar cells prepared under high relative humidity: Importance of PbI_2 morphology in two-step deposition of $CH_3NH_3PbI_3$. J. Mater. Chem. A **2015**, *3* (16), 8808–8815.
40. Burschka, J.; Pellet, N.; Moon, S.-J.; Humphry-Baker, R.; Gao, P.; Nazeeruddin, M.K.; Grätzel, M. Sequential deposition as a route to high-performance perovskite-sensitized solar cells. Nature **2013**, *499* (7458), 316–320.
41. Williams, S.T.; Rajagopal, A.; Chueh, C.C.; Jen, A.K.Y. Current challenges and prospective research for upscaling hybrid perovskite photovoltaics. J. Phys. Chem. Lett. **2016**, *7* (5), 811–819.
42. Jung, H.S.; Park, N.-G.G. Perovskite solar cells: From materials to devices. Small **2015**, *11* (1), 10–25.
43. Jeon, N.J.; Noh, J.H.; Kim, Y.C.; Yang, W.S.; Ryu, S.; Seok, S., II Solvent engineering for high-performance inorganic–organic hybrid perovskite solar cells. Nat. Mater. **2014**, *13* (9), 897–903.
44. Hu, H.; Wong, K.K.; Kollek, T.; Hanusch, F.; Polarz, S.; Docampo, P.; Schmidt-Mende, L. Highly efficient reproducible perovskite solar cells prepared by low-temperature processing. Molecules **2016**, *21* (4), 542.
45. Aldibaja, F.K.; Badia, L.; Mas-Marzá, E.; Sánchez, R.S.; Barea, E.M.; Mora-Sero, I. Effect of different lead precursors on perovskite solar cell performance and stability. J. Mater. Chem. A **2015**, *3* (17), 9194–9200.
46. Liu, D.; Gangishetty, M.K.; Kelly, T.L. Effect of $CH_3NH_3PbI_3$ thickness on device efficiency in planar heterojunction perovskite solar cells. J. Mater. Chem. A **2014**, *2* (46), 19873–19881.
47. Conings, B.; Baeten, L.; De Dobbelaere, C.; D'Haen, J.; Manca, J.; Boyen, H.-G. Perovskite-based hybrid solar cells exceeding 10% efficiency with high reproducibility using a thin film sandwich approach. Adv. Mater. **2014**, *26* (13), 2041–2046.
48. Ono, L.K.; Leyden, M.R.; Wang, S.; Qi, Y. Organometal halide perovskite thin films and solar cells by vapor deposition. J. Mater. Chem. A **2016**, *4* (18), 6693–6713.
49. Aidun, C.K.; Triantafillopoulos, N.G. High-speed blade coating. In *Liquid Film Coating*; Kistler, S.F., Schweizer, P.M., Eds.; Chapman & Hall: London, 1997; 637–672.
50. Yang, Z.; Chueh, C.C.; Zuo, F.; Kim, J.H.; Liang, P.W.; Jen, A.K.Y. High-performance fully printable perovskite solar cells via blade-coating technique under the ambient condition. Adv. Energy Mater. **2015**, *5* (13), 1500328.
51. Deng, Y.; Dong, Q.; Bi, C.; Yuan, Y.; Huang, J. Air-stable, efficient mixed-cation perovskite solar cells with Cu electrode by scalable fabrication of active layer. Adv. Energy Mater. **2016**, *6* (11), 1600372.
52. Deng, Y.; Wang, Q.; Yuan, Y.; Huang, J. Vividly colorful hybrid perovskite solar cells by doctor-blade coating with perovskite photonic nanostructures. Mater. Horizons **2015**, *2* (6), 578–583.
53. Murugadoss, G.; Thangamuthu, R.; Senthil Kumar, S.M. Fabrication of $CH_3NH_3PbI_3$ perovskite-based solar cells: Developing various new solvents for CuSCN hole transport material. Sol. Energy Mater. Sol. Cells **2017**, *164*, 56–62.
54. Sepalage, G.A.; Meyer, S.; Pascoe, A.; Scully, A.D.; Huang, F.; Bach, U.; Cheng, Y.B.; Spiccia, L. Copper(I) iodide as hole-conductor in planar perovskite solar cells: Probing the origin of J-V hysteresis. Adv. Funct. Mater. **2015**, *25* (35), 5650–5661.
55. Mohamad, D.K.; Griffin, J.; Bracher, C.; Barrows, A.T.; Lidzey, D.G. Spray-cast multilayer organometal perovskite solar cells fabricated in air. Adv. Energy Mater. **2016**, *6* (22), 1600994.
56. Habibi, M.; Rahimzadeh, A.; Bennouna, I.; Eslamian, M. Defect-free large-area (25 cm^2) light absorbing perovskite thin films made by spray coating. Coatings **2017**, *7* (3), 42.
57. Hwang, K.; Jung, Y.S.; Heo, Y.J.; Scholes, F.H.; Watkins, S.E.; Subbiah, J.; Jones, D.J.; Kim, D.Y.; Vak, D. Toward large scale roll-to-roll production of fully printed perovskite solar cells. Adv. Mater. **2015**, *27* (7), 1241–1247.
58. Razza, S.; Castro-Hermosa, S.; Di Carlo, A.; Brown, T.M. Research update: Large-area deposition, coating, printing, and processing techniques for the upscaling of perovskite solar cell technology. APL Mater. **2016**, *4* (9), 91508.
59. Muniz, E.C.; Góes, M.S.; Silva, J.J.; Varela, J.A.; Joanni, E.; Parra, R.; Bueno, P.R. Synthesis and characterization of mesoporous TiO_2 nanostructured films prepared by a modified sol–gel method for application in dye solar cells. Ceram. Int. **2011**, *37* (3), 1017–1024.
60. Ku, Z.; Rong, Y.; Xu, M.; Liu, T.; Han, H. Full printable processed mesoscopic $CH_3NH_3PbI_3/TiO_2$ heterojunction solar cells with carbon counter electrode. Sci. Rep. **2013**, *3* (1), 3132.
61. Zhang, L.; Liu, T.; Liu, L.; Hu, M.; Yang, Y.; Mei, A.; Han, H. The effect of carbon counter electrodes on fully printable mesoscopic perovskite solar cells. J. Mater. Chem. A **2015**, *3* (17), 9165–9170.
62. Yang, Y.; Ri, K.; Mei, A.; Liu, L.; Hu, M.; Liu, T.; Li, X.; Han, H. The size effect of TiO_2 nanoparticles on a printable mesoscopic perovskite solar cell. J. Mater. Chem. A **2015**, *3* (17), 9103–9107.
63. Cao, K.; Zuo, Z.; Cui, J.; Shen, Y.; Moehl, T.; Zakeeruddin, S.M.; Grätzel, M.; Wang, M. Efficient screen printed perovskite solar cells based on mesoscopic TiO_2/Al_2O_3/NiO/carbon architecture. Nano Energy **2015**, *17*, 171–179.
64. Grancini, G.; Roldán-Carmona, C.; Zimmermann, I.; Mosconi, E.; Lee, X.; Martineau, D.; Narbey, S.; Oswald, F.; De Angelis, F.; Graetzel, M.; Nazeeruddin, M.K. One-year stable perovskite solar cells by 2D/3D interface engineering. Nat. Commun. **2017**, *8*, 15684.
65. Sonavane, A.C.; Inamdar, A.I.; Shinde, P.S.; Deshmukh, H.P.; Patil, R.S.; Patil, P.S. Efficient electrochromic nickel oxide thin films by electrodeposition. J. Alloys Compd. **2010**, *489* (2), 667–673.
66. Su, T.-S.; Hsieh, T.-Y.; Hong, C.-Y.; Wei, T.-C. Electrodeposited ultrathin TiO_2 blocking layers for efficient perovskite solar cells. Sci. Rep. **2015**, *5*, 16098.
67. Koza, J.A.; Hill, J.C.; Demster, A.C.; Switzer, J.A. Epitaxial electrodeposition of methylammonium lead iodide perovskites. Chem. Mater. **2016**, *28* (1), 399–405.
68. Huang, J.; Jiang, K.; Cui, X.; Zhang, Q.; Gao, M.; Su, M.; Yang, L.; Song, Y. Direct conversion of $CH_3NH_3PbI_3$ from electrodeposited PbO for highly efficient planar perovskite solar cells. Sci. Rep. **2015**, *5*, 15889.

69. Chen, H.; Wei, Z.; Zheng, X.; Yang, S. A scalable electrodeposition route to the low-cost, versatile and controllable fabrication of perovskite solar cells. Nano Energy **2015**, *15*, 216–226.
70. Cameron, N.L. Ink-jet printing. In *Coatings Technology Fundamentals, Testing, and, Processing Techniques*; Tracton, A.A., Ed.; Taylor and Francis Group: Boca Raton, FL, 2007.
71. Calvert, P. Inkjet printing for materials and devices. Chem. Mater. **2001**, *13* (10), 3299–3305.
72. Teichler, A.; Perelaer, J.; Schubert, U.S. Inkjet printing of organic electronics—Comparison of deposition techniques and state-of-the-art developments. J. Mater. Chem. C **2013**, *1* (10), 1910–1925.
73. Li, S.-G.; Jiang, K.-J.; Su, M.-J.; Cui, X.-P.; Huang, J.-H.; Zhang, Q.-Q.; Zhou, X.-Q.; Yang, L.-M.; Song, Y.-L. Inkjet printing of $CH_3NH_3PbI_3$ on a mesoscopic TiO_2 film for highly efficient perovskite solar cells. J. Mater. Chem. A **2015**, *3* (17), 9092–9097.
74. Jiang, Z.; Bag, M.; Renna, L.; Jeong, S.P.; Rotello, V.; Venkataraman, D. Aqueous-processed perovskite solar cells based on reactive inkjet printing. Hal **2016**, *1*, hal–01386295.
75. Mathies, F.; Abzieher, T.; Hochstuhl, A.; Glaser, K.; Colsmann, A.; Paetzold, U.W.; Hernandez-Sosa, G.; Lemmer, U.U.; Quintilla, A.; Rueda, D.; Quintilla, A.; Lemmer, U.U. Multipass inkjet printed planar methylammonium lead iodide perovskite solar cells. J. Mater. Chem. A **2016**, *4* (48), 19207–19213.
76. Wei, Z.; Chen, H.; Yan, K.; Yang, S. Inkjet printing and instant chemical transformation of a $CH_3NH_3PbI_3$/nanocarbon electrode and interface for planar perovskite solar cells. Angew. Chem. Int. Ed. **2014**, *53* (48), 13239–13243.
77. Huang, W.; Manser, J.S.; Kamat, P.V.; Ptasinska, S. Evolution of chemical composition, morphology, and photovoltaic efficiency of $CH_3NH_3PbI_3$ perovskite under ambient conditions. Chem. Mater. **2016**, *28* (1), 303–311.
78. Niu, G.; Li, W.; Meng, F.; Wang, L.; Dong, H.; Qiu, Y. Study on the stability of $CH_3NH_3PbI_3$ films and the effect of post-modification by aluminum oxide in all-solid-state hybrid solar cells. J. Mater. Chem. A **2014**, *2* (3), 705–710.
79. Christians, J.A.; Miranda Herrera, P.A.; Kamat, P.V. Transformation of the excited state and photovoltaic efficiency of $CH_3NH_3PbI_3$ perovskite upon controlled exposure to humidified air. J. Am. Chem. Soc. **2015**, *137* (4), 1530–1538.
80. Leguy, A.M.A.; Hu, Y.; Campoy-Quiles, M.; Alonso, M.I.; Weber, O.J.; Azarhoosh, P.; van Schilfgaarde, M.; Weller, M.T.; Bein, T.; Nelson, J.; Docampo, P.; Barnes, P.R.F. Reversible hydration of $CH_3NH_3PbI_3$ in films, single crystals, and solar cells. Chem. Mater. **2015**, *27* (9), 3397–3407.
81. Sheng, R.; Wen, X.; Huang, S.; Hao, X.; Chen, S.; Jiang, Y.; Deng, X.; Green, M.A.; Ho-Baillie, A. Photoluminescence characterisations of a dynamic aging process of organic–inorganic $CH_3NH_3PbBr_3$ perovskite. Nanoscale **2016**, *8* (4), 1926–1931.
82. Bella, F.; Griffini, G.; Correa-Baena, J.-P.; Saracco, G.; Gratzel, M.; Hagfeldt, A.; Turri, S.; Gerbaldi, C. Improving efficiency and stability of perovskite solar cells with photocurable fluoropolymers. Science **2016**, *354* (6309), 203–206.
83. Niu, G.; Li, W.; Li, J.; Liang, X.; Wang, L.; D'Olieslaeger, L.; Ethirajan, A.; Berbeeck, J.; Manca, J.; Mosconi, E.; Angelis, F.D.; Boyen, H.-G.; Ginger, D.S.; Friend, R.H.; Snaith, H.J. Enhancement of thermal stability for perovskite solar cells through cesium doping. RSC Adv. **2017**, *7* (28), 17473–17479.
84. Jeon, N.J.; Noh, J.H.; Yang, W.S.; Kim, Y.C.; Ryu, S.; Seo, J.; Seok, S., II Compositional engineering of perovskite materials for high-performance solar cells. Nature **2015**, *517* (7535), 476–480.
85. Supasai, T.; Rujisamphan, N.; Ullrich, K.; Chemseddine, A.; Dittrich, T. Formation of a passivating $CH_3NH_3PbI_3$/PbI_2 interface during moderate heating of $CH_3NH_3PbI_3$ layers. Appl. Phys. Lett. **2013**, *103* (18), 183906.
86. Dualeh, A.; Tétreault, N.; Moehl, T.; Gao, P.; Nazeeruddin, M.K.; Grätzel, M. Effect of annealing temperature on film morphology of organic-inorganic hybrid pervoskite solid-state solar cells. Adv. Funct. Mater. **2014**, *24* (21), 3250–3258.
87. Conings, B.; Drijkoningen, J.; Gauquelin, N.; Babayigit, A.; D'Haen, J.; D'Olieslaeger, L.; Ethirajan, A.; Verbeeck, J.; Manca, J.; Mosconi, E.; De Angelis, F.; Boyen, H.G. Intrinsic thermal instability of methylammonium lead trihalide perovskite. Adv. Energy Mater. **2015**, *5* (15), 1500477.
88. Sutton, R.J.; Eperon, G.E.; Miranda, L.; Parrott, E.S.; Kamino, B.A.; Patel, J.B.; Hrantner, M.T.; Johnston, M.B.; Haghighirad, A.A.; Moore, D.T.; Snaith, H.J. Bandgap-tunable cesium lead halide perovskites with high thermal stability for efficient solar cells. Adv. Energy Mater. **2016**, *6* (8), 1502458.
89. Lee, J.W.; Kim, D.H.; Kim, H.S.; Seo, S.W.; Cho, S.M.; Park, N.G. Formamidinium and cesium hybridization for photo- and moisture-stable perovskite solar cell. Adv. Energy Mater. **2015**, *5* (20), 1501310.
90. Leijtens, T.; Eperon, G.E.; Pathak, S.; Abate, A.; Lee, M.M.; Snaith, H.J. Overcoming ultraviolet light instability of sensitized TiO_2 with meso-superstructured organometal tri-halide perovskite solar cells. Nat. Commun. **2013**, *4*, 28885.
91. Nie, W.; Blancon, J.C.; Neukirch, A.J.; Appavoo, K.; Tsai, H.; Chhowalla, M.; Alam, M.A.; Sfeir, M.Y.; Katan, C.; Even, J.; Tretiak, S.; Crochet, J.J.; Gupta, G.; Mohite, A.D. Light-activated photocurrent degradation and self-healing in perovskite solar cells. Nat. Commun. **2016**, *7*, 11574.
92. Ahn, N.; Kwak, K.; Jang, M.S.; Yoon, H.; Yang, B.; Lee, J.; Pikhitsa, P.V.; Byun, J.; Choi, M. Trapped charge driven degradation of perovskite solar cells. Nat. Commun. **2016**, *7*, 13422.
93. Tan, H.; Jain, A.; Voznyy, O.; Lan, X.; García de Arquer, F.P.; Fan, J.Z.; Quintero-Bermudez, R.; Yuan, M.; Zhang, B.; Zhao, Y.Y.; Fan, F.; Li, P.; Quan, L.N.; Zhao, Y.Y.; Lu, Z.-H.; Yang, Z.; Hoogland, S.; Sargent, E.H. Efficient and stable solution-processed planar perovskite solar cells via contact passivation. Science **2017**, *355* (6326), 722–726.
94. Li, Y.; Zhao, Y.; Chen, Q.; Yang, Y.; Liu, Y.; Hong, Z.; Liu, Z.; Hsieh, Y.T.; Meng, L.; Li, Y.; Yang, Y. Multifunctional fullerene derivative for interface engineering in perovskite solar cells. J. Am. Chem. Soc. **2015**, *137* (49), 15540–15547.

95. Abrusci, A.; Stranks, S.D.; Docampo, P.; Yip, H.L.; Jen, A.K.Y.; Snaith, H.J. High-performance perovskite-polymer hybrid solar cells via electronic coupling with fullerene monolayers. Nano Lett. **2013**, *13* (7), 3124–3128.
96. Wojciechowski, K.; Stranks, S.D.; Abate, A.; Sadoughi, G.; Sadhanala, A.; Kopidakis, N.; Rumbles, G.; Li, C.-Z.; Friend, R.H.; Jen, A.K.-Y.; Snaith, H.J. Heterojunction modification for highly efficient organic–inorganic perovskite solar cells. ACS Nano **2014**, *8* (12), 12701–12709.
97. Xiao, Z.; Yuan, Y.; Shao, Y.; Wang, Q.; Dong, Q.; Bi, C.; Sharma, P.; Gruverman, A.; Huang, J. Giant switchable photovoltaic effect in organometal trihalide perovskite devices. Nat. Mater. **2014**, *14* (2), 193–198.
98. Elumalai, N.K.; Uddin, A. Hysteresis in organic-inorganic hybrid perovskite solar cells. Sol. Energy Mater. Sol. Cells **2016**, *157*, 476–509.
99. Chen, B.; Yang, M.; Priya, S.; Zhu, K. Origin of J-V hysteresis in perovskite solar cells. J. Phys. Chem. Lett. **2016**, *7* (5), 905–917.
100. Calado, P.; Telford, A.M.; Bryant, D.; Li, X.; Nelson, J.; O'Regan, B.C.; Barnes, P.R.F. Evidence for ion migration in hybrid perovskite solar cells with minimal hysteresis. Nat. Commun. **2016**, *7*, 13831.
101. Van Reenen, S.; Kemerink, M.; Snaith, H.J. Modeling anomalous hysteresis in perovskite solar cells. J. Phys. Chem. Lett. **2015**, *6* (19), 3808–3814.
102. Zhang, T.; Chen, H.; Bai, Y.; Xiao, S.; Zhu, L.; Hu, C.; Xue, Q.; Yang, S. Understanding the relationship between ion migration and the anomalous hysteresis in high-efficiency perovskite solar cells: A fresh perspective from halide substitution. Nano Energy **2016**, *26*, 620–630.
103. Zhang, J.; Gao, X.; Deng, Y.; Zha, Y.; Yuan, C. Comparison of life cycle environmental impacts of different perovskite solar cell systems. Sol. Energy Mater. Sol. Cells **2017**, *166*, 9–17.
104. Serrano-Lujan, L.; Espinosa, N.; Larsen-Olsen, T.T.; Abad, J.; Urbina, A.; Krebs, F.C. Tin- and lead-based perovskite solar cells under scrutiny: An environmental perspective. Adv. Energy Mater. **2015**, *5* (20), 1501119.